

## Quantum rotor atoms in light beams with orbital angular momentum: Highly accurate rotation sensor

Igor Kuzmenko,<sup>1,2,3</sup> Tetyana Kuzmenko,<sup>1,3</sup> and Yehuda B. Band<sup>1,2,3,4</sup>

<sup>1</sup>*Department of Physics, Ben-Gurion University of the Negev, Beer-Sheva 84105, Israel*

<sup>2</sup>*Department of Chemistry, Ben-Gurion University of the Negev, Beer-Sheva 84105, Israel*

<sup>3</sup>*The Ilse Katz Center for Nano-Science, Ben-Gurion University of the Negev, Beer-Sheva 84105, Israel*

<sup>4</sup>*Department of Electro-Optics, Ben-Gurion University of the Negev, Beer-Sheva 84105, Israel*



(Received 19 March 2020; accepted 14 December 2020; published 30 December 2020)

Atoms trapped in a red-detuned retroreflected Laguerre-Gaussian beam undergo orbital motion within rings whose centers are on the axis of the laser beam. We determine the wave functions, energies, and degeneracies of such quantum rotors (QRs), and the microwave transitions between the energy levels. We then show how such QR atoms can be used as highly accurate rotation sensors when the rings are singly occupied.

DOI: [10.1103/PhysRevA.102.063127](https://doi.org/10.1103/PhysRevA.102.063127)

### I. INTRODUCTION

We demonstrate that quantum rotor (QR) atoms (atoms whose motion is constrained to a circular ring [1]) form bound motional states in light beams having orbital angular momentum, and that they can be used as an extremely high-accuracy rotation sensor. More precisely, QR atoms can be trapped in a red-detuned linearly polarized retroreflected Laguerre-Gaussian (LG) beam [2–7], and *singly occupied rings* can be configured [8–10] (see Fig. 1) and used as a rotation sensor. Single occupation and negligible tunneling between rings [11] are important to suppress deleterious spin-exchange collisions between QR atoms for sensor applications. The accuracy estimate obtained here suggests that this may be the highest-precision rotation sensor proposed to date.

Atoms trapped in light beams having orbital angular momentum have been studied theoretically [2,12,13] and experimentally [5,11,14]. Atoms trapped in two co- and counterpropagating LG beams with *opposite* orbital angular momentum,  $l$  and  $-l$ , were considered in Ref. [2]. In the case of copropagating beams, the intensity of the light field is proportional to  $\cos^2(l\phi)$ , where  $\phi$  is the angle around the beam axis, which is taken to be the  $z$  axis. This leads to the appearance of  $2l$  petal-like high-intensity regions around the beam axis, and the trapped atoms move along the axis of the LG beams [2]. In the counterpropagating case, the light intensity is proportional to  $\cos^2(l\phi - kz)$ , where  $k$  is the laser wave number, and the laser beams form helical optical tubes. If the light is red detuned from atomic resonance, atoms are trapped within the helical tubes that twist about the axis of the beams [2]. The characteristics of atoms trapped in red-detuned LG retroreflected beams, with light intensity proportional to  $\cos^2(kz)$  (no  $\phi$  dependence—see below), still need to be studied. We calculate the motional eigenfunctions and eigenenergies of such atoms, and show that such atoms can be used as a highly accurate rotation sensor.

Atomic gyroscopes are studied in Refs. [15–18]. There are two types of atomic gyroscopes: atomic interferometer

gyroscopes, which utilize the atomic interferometer to sense rotation, and atomic spin gyroscopes, which utilize atomic spin to sense rotation. The highest atomic gyro sensitivity reported is for an atomic interferometer gyroscope. The sensitivity reported was  $10^{-7}$  rad s $^{-1}$  Hz $^{-1/2}$ , and the stability 1 nrad/s after  $10^4$  s of integration time [15]. Here, we show that an accuracy of QR rotation sensors can reach  $4.8 \times 10^{-10}$  s $^{-1}$ , using  $N = 161$  QRs of radius  $r_l = 15.81$   $\mu$ m. This can be improved by increasing  $r_l$  and  $N$ .

The outline of this paper is as follows. LG beams with orbital angular momentum, and in particular, retroreflected LG beams, are described in Sec. II. Wave functions and energies of trapped atoms are calculated in Sec. III, and we show that the trapped atoms are QRs. The Ramsey separated field method [19] with microwave Raman pulses is developed in Sec. IV. In Sec. V we show how the QRs can be used as rotation sensors. Rabi oscillations in the rotating frame of reference are described in Sec. V A, and the accuracy of the QR rotation sensor is estimated in Sec. V B. Section V C discusses the measurement of the angular velocity in the case when gravity is present. The results are summarized in Sec. VI.

### II. RETROREFLECTED LAGUERRE-GAUSSIAN BEAMS

An LG beam propagating along the  $z$  axis with orbital angular momentum  $l$  and polarization  $\mathbf{e}_\alpha$  can be written in terms of a slowly varying envelope  $u_{l,p}(r, \phi, z)$  of the electric field as

$$\mathbf{E}_{\alpha,l,p}(\mathbf{r}, t) = u_{l,p}(r, \phi, z) e^{i(kz - k_0 z_0 - \omega t)} \mathbf{e}_\alpha + \text{c.c.}, \quad (1)$$

where the field amplitude mode  $\text{LG}_p^l(\mathbf{r}) \equiv u_{l,p}(\mathbf{r})$  in SI units is [2–7]

$$\begin{aligned} u_{l,p}(r, \phi, z) &= \sqrt{\frac{2p!}{\pi(p+|l|)!}} \frac{\sqrt{P_0/(c\epsilon_0)}}{w(z)} \left(\frac{r\sqrt{2}}{w(z)}\right)^{|l|} \exp\left(-\frac{r^2}{w^2(z)}\right) \end{aligned}$$

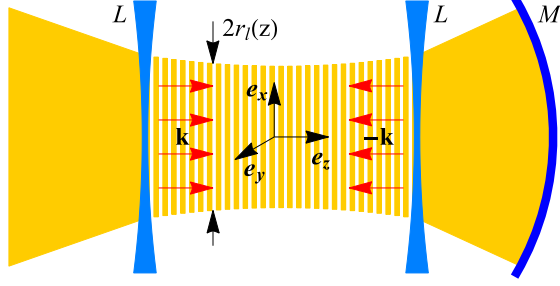


FIG. 1. Two lenses ( $L$ ) refract the LG beam (orange region). The mirror ( $M$ ) reflects the beam, and two counterpropagating beams result. An almost uniform beam waist  $w_0$  exists between the lenses [radii  $r_l(z)$  of the rings depend only weakly on  $z$ ]. The wave vectors of the incident and reflected beams are  $\pm\mathbf{k}$ . A series of ring optical potentials are stacked perpendicular to the beam axis. White and orange denote potential minima and maxima of the light intensity, respectively.  $\mathbf{e}_x$ ,  $\mathbf{e}_y$ , and  $\mathbf{e}_z$  are unit vectors in the  $x$ ,  $y$ , and  $z$  axes, and  $[r_l(z_j), z_j]$  are minima of the potential energy.

$$\begin{aligned} & \times L_p^{||l|} \left( \frac{2r^2}{w^2(z)} \right) \exp \left( -\frac{ikr^2z}{2(z^2 + z_R^2)} \right) \exp(-il\phi) \\ & \times \exp \left[ i(2p + |l| + 1) \tan^{-1} \left( \frac{z}{z_R} \right) \right]. \end{aligned} \quad (2)$$

Here,  $z$  is the longitudinal distance from the beam focus located at  $z = 0$ ,  $P_0$  is the laser beam power,  $\epsilon_0$  is the vacuum permittivity,  $w_0$  is the beam waist at  $z = 0$ ,  $w(z) = w_0[1 + (z/z_R)^2]^{1/2}$  is the radius at which the beam intensity falls to  $1/e$  of its axis value at  $z$ , and  $z_R = \pi w_0^2/\lambda$  is the Rayleigh range for the laser with wavelength  $\lambda = 2\pi/k$ , where  $k = \omega/c$  is the wave number,  $0 < z_0 < \lambda/2$  is a phase parameter,  $L_p^{||l|}(x)$  is the associated Laguerre polynomial,  $\phi$  is the azimuthal angle, and  $\tan^{-1}(z/z_R)$  is the Gouy phase. Figure 1 is a schematic diagram of a retroreflected LG beam propagating along the  $z$  axis. It shows the superposition of two counterpropagating beams that form a standing wave along the  $z$  axis. The electric field of the counterpropagating (cp) standing wave has the form

$$\begin{aligned} \mathbf{E}_{\alpha,l,p}^{\text{cp}}(\mathbf{r}, t) &= u_{l,p}(r, \phi, z) \mathbf{e}_\alpha (e^{i(kz - kz_0 - \omega t)} \\ &+ e^{i(-kz + kz_0 - \omega t)}) + \text{c.c.} \end{aligned} \quad (3)$$

This standing-wave configuration results in a series of ring-shaped optical potentials (orange stripes in Fig. 1) stacked perpendicular to the beam axis. Since our interest is in trapping atoms in the light beam, the light frequency is red detuned from atomic resonance. Atoms will be trapped in the ring-shaped optical potentials.

### III. QR BOUND STATES IN LG RINGS

Consider atoms trapped in the counterpropagating linearly polarized LG beams of Eq. (3). The QR Hamiltonian operator in cylindrical coordinates is

$$H = -\frac{\hbar^2}{2M} \left( \frac{\partial^2}{\partial r^2} + \frac{1}{r} \frac{\partial}{\partial r} + \frac{1}{r^2} \frac{\partial^2}{\partial \phi^2} + \frac{\partial^2}{\partial z^2} \right) + V(\mathbf{r}), \quad (4)$$

where the first term is the atom kinetic energy expressed in polar coordinates and  $V(\mathbf{r})$  is the optical potential resulting from the LG beams, which is calculated as a second-order ac Stark shift [20] in the rotating-wave approximation [21,22] and is given in terms of the ac polarizability  $\alpha(\omega)$  by  $V(\mathbf{r}) = -\alpha(\omega) |\mathbf{E}_{\alpha,l,p}^{\text{cp}}(\mathbf{r}, t)|^2$ . In the standing-wave configuration in the nearly constant beam waist region between the lenses, the optical potential can be taken to be two dimensional since the widths of the rings are very small. For an  $\text{LG}_0^l$  mode ( $p = 0$  and  $l \neq 0$ ), the potential is  $\phi$  independent,

$$V(r, z) = -V_0 \cos^2 [k(z - z_0)] \frac{\rho^{2||l|}(z)}{\mathfrak{w}^2(z)} e^{-||l|\rho^2(z)-1|}, \quad (5)$$

where  $\rho(z) = r/r_l(z)$ ,  $\mathfrak{w}(z) = w(z)/w_0$ , and  $V_0 = \frac{\alpha(\omega)P_0}{c w_0^2} \frac{2^{|l|}}{\pi^{|l|}} e^{-l}$ . Potential (5) has minima at

$$z = z_j \equiv \frac{\pi}{k} j + z_0, \quad r = r_l(z_j) \equiv w(z_j) \sqrt{|l|/2}, \quad (6)$$

where  $j$  is an integer, and the trapped atoms execute circular motion around the  $z$  axis within the minima, i.e., they are QRs.  $V[r_l(z_j), z_j]$  is given by  $V[r_l(z_j), z_j] = -V_0[w_0/w(z_j)]^2$ . For  $z$  close to  $z_j$ ,

$$V(r, z) \approx V_l(r) + W_j(z), \quad (7)$$

where

$$V_l(r) = V(r, z_j), \quad W_j(z) = \frac{V_0 k^2}{\mathfrak{w}^2(z_j)} (z - z_j)^2. \quad (8)$$

$W_j(z)$  is a harmonic potential in  $z - z_j$ , and the corresponding harmonic frequency and length are

$$\omega_z(z_j) = \frac{2}{\mathfrak{w}(z_j)} \frac{\sqrt{\mathcal{E}_0 V_0}}{\hbar}, \quad b_z(z_j) = \frac{\sqrt{\mathfrak{w}(z_j)}}{k} \left( \frac{\mathcal{E}_0}{V_0} \right)^{1/4}, \quad (9)$$

where  $\mathcal{E}_0 = \hbar^2 k^2 / (2M)$  is the recoil energy.

The optical potential (5) is invariant with respect to rotations about the  $z$  axis, therefore the quantum states of the QR in the harmonic approximation (7) are parametrized by radial and vertical quantum numbers  $n_r$  and  $n_z$  describing radial and  $z$  motion ( $n_r, n_z = 0, 1, 2, \dots$ ), the orbital momentum quantum number  $m_\ell$ , and the projection  $m_F$  of the hyperfine angular momentum  $\mathbf{F}$  on the  $z$  axis. The ground state has  $n_z = n_r = m_\ell = 0$ , and is  $2F + 1$ -fold degenerate. Orbitorially excited states with  $m_\ell \neq 0$  are  $2(2F + 1)$ -fold degenerate, and have angular momentum  $\pm m_\ell$ . Radial and vertical excitations have  $n_r \neq 0$  and  $n_z \neq 0$ , respectively.

For simplicity, in this paragraph, let us consider an atom trapped at the  $z_0$  site (i.e., near  $z_j$  with  $j = 0$ ). The QR wave functions and eigenenergies satisfy the Schrödinger equation,

$$\left[ -\frac{\hbar^2}{2M} \nabla^2 + V(r, z) - \epsilon_n \right] \Psi_{\mathbf{n}}(\mathbf{r}) = 0, \quad (10)$$

where  $\mathbf{n} = (n_z, n_r, m_\ell)$ . The wave function can be written in cylindrical coordinates  $\mathbf{r} = (r, \phi, z)$  as

$$\Psi_{\mathbf{n}}(\mathbf{r}) = \frac{1}{\sqrt{2\pi}} \eta_{n_z}(z) \psi_{n_r, m_\ell}(r) e^{im_\ell \phi}, \quad (11)$$

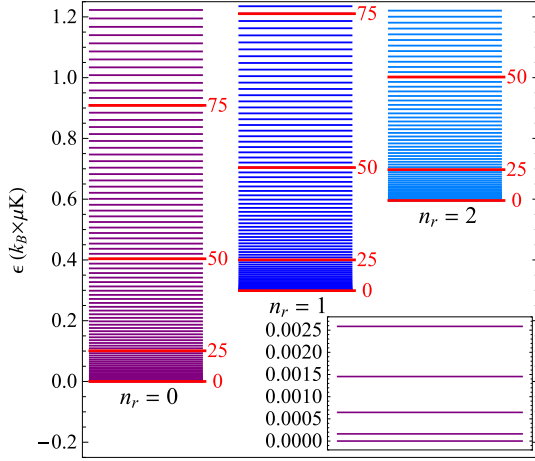


FIG. 2. Energies  $\epsilon(n_z, n_r, m_\ell)$  of a  ${}^6\text{Li}$  QR (relative to the QR ground-state energy) trapped in an LG beam with  $\lambda = 1064$  nm,  $w_0 = 10 \mu\text{m}$ ,  $l = 5$ ,  $p = 0$ , and  $V_0 = 10\mathcal{E}_0$ , where  $\mathcal{E}_0 = k_B \times 1.40612 \mu\text{K}$  is the recoil energy. This gives  $r_l \equiv r(z=0)$  equal to  $15.81 \mu\text{m}$ . Energies with  $n_r = 0$  are shown as purple lines,  $n_r = 1$  as blue lines, and  $n_r = 2$  as azure lines. The red lines show the levels with  $m_\ell = 0, 25, 50$ , and  $75$ , respectively. The inset shows  $\epsilon(0, 0, m_\ell)$  with  $|m_\ell| \leq 4$ . Quantum states with  $n_z \geq 1$  have high energies and fall out of the scale of the figure, hence only  $n_z = 0$  are shown.

where  $\eta_{n_z}(z)$  and  $\psi_{n_r, m_\ell}(r)$  satisfy the equations

$$\left[ -\frac{\hbar^2}{2M} \frac{d^2}{dz^2} + W_0(z) - \epsilon_z(n_z) \right] \eta_{n_z}(z) = 0, \quad (12)$$

$$\left[ -\frac{\hbar^2}{2Mr} \frac{d}{dr} \left( r \frac{d}{dr} \right) + V_l(r) + m_\ell^2 C(r) - \epsilon_r(n_r, m_\ell) \right] \psi_{n_r, m_\ell}(r) = 0. \quad (13)$$

$V_l(r)$  and  $W_j(z)$  are given by Eq. (8), and  $C(r) = \frac{\hbar^2}{2Mr^2}$  is the rotational (centrifugal) energy of the QR around the  $z$  axis. The eigenenergy of the trapped atom is  $\epsilon(\mathbf{n}) = \epsilon_z(n_z) + \epsilon_r(n_r, m_\ell)$ , and the QR vertical, radial, and orbital excitation energies are  $\epsilon_z = \epsilon_z(1) - \epsilon_z(0) \approx \hbar\omega_z$ ,  $\epsilon_r = \epsilon_r(1, 0) - \epsilon_r(0, 0)$ ,  $\epsilon_\ell = \epsilon_r(0, 1) - \epsilon_r(0, 0) \approx C(r_l)$ . We assume they satisfy the inequalities

$$\epsilon_z \gg \epsilon_r \gg \epsilon_\ell, \quad (14)$$

i.e., the orbital excitations are the lowest-energy excitations and the radial and longitudinal modes have higher energies.

The Schrödinger equation (13) for the radial degree of freedom of the trapped atoms contains the effective potential  $V_l(r) + m_\ell^2 C(r)$ , where  $V_l(r)$  is given by Eq. (8), and  $m_\ell$  is an integer. The potential  $V_l(r)$  has a minimum at  $r = r_l$  given by Eq. (6), and can be well approximated by a harmonic oscillator near  $r = r_l$ . The weak centrifugal energy  $C(r)$  slightly changes the equilibrium position and harmonic frequency of the radial motion.

The numerically calculated energy eigenvalues  $\epsilon_r(n_r, m_\ell)$  for  ${}^6\text{Li}$  QR atoms are shown in Fig. 2 for  $l = 5$ ,  $w_0 = 10 \mu\text{m}$ ,  $r_l = 15.81 \mu\text{m}$ , and  $V_0 = 10\mathcal{E}_0 = k_B \times 14.0612 \mu\text{K}$ . The excitation energies  $\epsilon_r(0, m_\ell) - \epsilon_r(0, 0)$  with  $|m_\ell| \leq 100$

are approximated by

$$\epsilon_r(0, m_\ell) - \epsilon_r(0, 0) = [a_2 m_\ell^2 - a_4 m_\ell^4] C(r_l), \quad (15)$$

where  $a_2 = 1.00097$  and  $a_4 = 1.12 \times 10^{-6}$ . It is seen that  $\epsilon_r(0, m_\ell) - \epsilon_r(0, 0) \approx m_\ell^2 C(r_l)$ . For example,

$$\begin{aligned} \epsilon_r(0, 1) - \epsilon_r(0, 0) &= 1.0011 C(r_l) \\ &= 0.1615 \text{ nK}. \end{aligned} \quad (16)$$

The slight difference of  $\epsilon_r(0, 1) - \epsilon_r(0, 0)$  from  $m_\ell^2 C(r_l)$  is due to the finite thickness of the quantum rotor. Moreover, the inequality

$$\frac{\epsilon_r(0, m_\ell) - \epsilon_r(0, 0)}{\epsilon_r(0, 1) - \epsilon_r(0, 0)} = m_\ell^2 \left[ 1 - \frac{a_4(m_\ell^2 - 1)}{a_2 - a_4} \right] \lesssim m_\ell^2$$

indicates the small shift of the equilibrium position for the potential  $V_l(r) + m_\ell^2 C(r)$  with respect to the equilibrium position  $r_l$  for the potential  $V_l(r)$ . The excitation energies  $\epsilon_r(n_r, 0) - \epsilon_r(0, 0)$  are

$$\begin{aligned} \epsilon_r(1, 0) - \epsilon_r(0, 0) &= 1853 C(r_l), \\ \epsilon_r(2, 0) - \epsilon_r(0, 0) &= 3692 C(r_l). \end{aligned} \quad (17)$$

The excitation energies  $\epsilon_r(2, 0) - \epsilon_r(0, 0)$  are very nearly equal to  $2[\epsilon_r(1, 0) - \epsilon_r(0, 0)]$ ; the harmonic approximation for the radial excitations is valid for relatively small  $n_r$ .

The energies calculated from Eq. (12) are

$$\epsilon_z(0) = 2.757 \times 10^4 C(r_l), \quad \epsilon_z(1) = 8.271 \times 10^4 C(r_l),$$

and the excitation energy is

$$\epsilon_z(1) - \epsilon_z(0) = 5.514 \times 10^4 C(r_l). \quad (18)$$

Equations (16)–(18) show that the inequality (14) is satisfied.

#### IV. RABI OSCILLATION METHOD WITH RAMAN PULSES

In order to measure the excitation energies of the QR atoms with quantum numbers  $n_r$ ,  $m_\ell$ , and  $m_F$ , we propose to subject the QRs to three pulses, as shown in Fig. 3(a). We use pump and Stokes microwave-frequency pulses with frequencies  $\omega_p \gtrsim \omega_s$ , that are detuned from the quantum transition between the hyperfine states of the ground state [see Fig. 3(b)], and an LG pulse with frequency  $\omega_e$  far detuned from the resonant frequency of the  ${}^2S_{1/2} \rightarrow {}^2P_{3/2}$  electronic transition [not explicitly shown in Fig. 3(b)]. The microwave-frequency pump and Stokes light cannot change the orbital quantum number  $m_\ell$ , but the LG pulse allows transitions  $|m_\ell\rangle \rightarrow |m'_\ell\rangle$  between quantum states with different orbital quantum numbers  $m_\ell$  and  $m'_\ell$  [as shown in Fig. 3(b)]. The pump and Stokes pulses propagate parallel and antiparallel to the  $x$  axis and are linearly polarized with magnetic field polarization along the  $z$  axis. The pump and Stokes magnetic fields are given by

$$\begin{aligned} \mathbf{B}_\mu(\mathbf{r}, t) &= \mathbf{B}_\mu^{(0)} \cos(k_\mu x - \omega_\mu t) \Theta(t, \tau - t) \\ &\approx \mathbf{B}_\mu^{(0)} \cos(\omega_\mu t) \Theta(t, \tau - t), \end{aligned}$$

where  $\mu = p, s$  and we assume square pulses, hence the presence of the  $\Theta$  function which equals 1 for  $0 < t < \tau$  and is 0 elsewhere (i.e., both arguments must be positive for the  $\Theta$  function to be 1). Here, we take into account that the

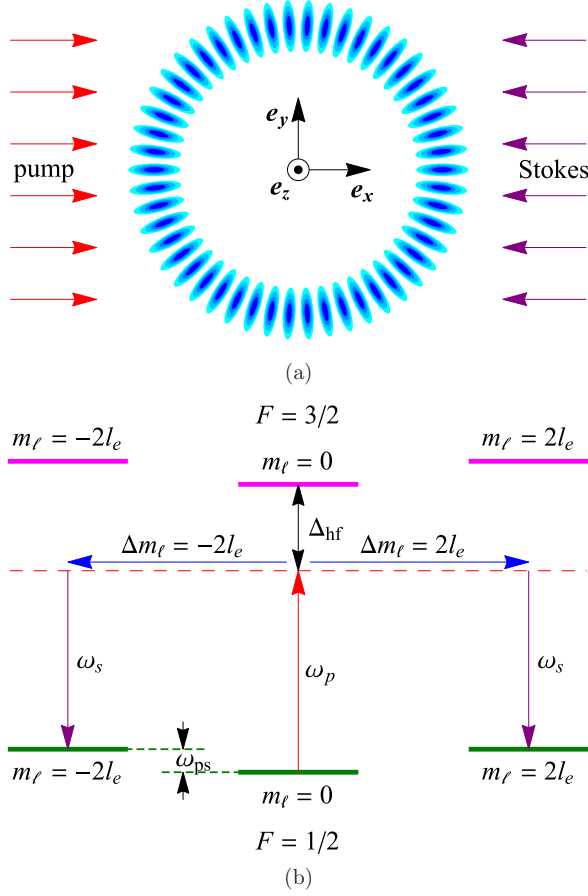


FIG. 3. (a) Pump and Stokes microwave-frequency pulses (red and purple arrows) and optical rotational counterpropagating LG rotational-kick pulses with  $l_e = 25$  (along the  $z$  axis). The blue regions indicate the depth of the rotational-kick LG pulse potential.  $\mathbf{e}_x$ ,  $\mathbf{e}_y$ , and  $\mathbf{e}_z$  are unit vectors along the  $x$ ,  $y$ , and  $z$  axes. (b) Quantum transitions due to the pump, Stokes, and rotational-kick pulses (red, purple, and blue arrows). The frequencies of the pump and Stokes pulses are  $\omega_p$  and  $\omega_s$ , and their difference  $\omega_{ps} = \omega_p - \omega_s$  is equal to the transition frequency  $\omega_{2L,0}$ . Detuning of  $\omega_p$  from the resonant frequency of the  ${}^2S_{1/2}(F=1/2)$  to  ${}^2S_{1/2}(F=3/2)$  quantum transition is  $\Delta_{\text{hf}}$ .

wavelengths  $\lambda_\mu$  are much longer than the radius  $r_l$  of the QR, hence  $\mathbf{B}_\mu$  depends on  $t$ , but not on  $\mathbf{r}$ . Therefore these pulses do not induce Raman transitions between the quantum states  $|n_r, m_\ell\rangle$  and  $|n'_r, m'_\ell\rangle$  and we can approximate  $\mathbf{B}_\mu(\mathbf{r}, t)$  by  $\mathbf{B}_\mu(t) \equiv \mathbf{B}_\mu(0, t)$ . Hence, the dipole magnetic interaction between the QR and the microwaves,

$$H_\mu = -g\mu_{BS} \cdot \mathbf{B}_\mu(t) \quad (19)$$

(where  $\mu = p, s$  for the pump and Stokes microwave pulses, and  $\mathbf{s}$  is a vector of the electronic spin- $\frac{1}{2}$  operators), does not depend on the position of the atom,  $\mathbf{r}$ . Moreover, we assume that  $\mathbf{B}_\mu^{(0)} = B_\mu^{(0)}\mathbf{e}_z$ , thus

$$\begin{aligned} &\langle {}^2S_{1/2}(F), n_r, m_\ell, m_F | H_\mu | {}^2S_{1/2}(F'), n'_r, m'_\ell, m'_F \rangle \\ &\times \propto \delta_{n_r, n'_r} \delta_{m_\ell, m'_\ell} \delta_{m_F, m'_F}, \end{aligned}$$

where  $|{}^2S_{1/2}(F), n_r, m_\ell, m_F\rangle$  describes the atom in the ground  ${}^2S_{1/2}$  state with hyperfine orbital angular momentum  $F$ , projection  $m_F$  of  $\mathbf{F}$  on the direction of  $\mathbf{B}_\mu^{(0)}$ , and radial and orbital quantum numbers of the QR  $n_r$  and  $m_\ell$ . For Raman transitions  $|{}^2S_{1/2}(F), n_r, m_\ell, m_F\rangle \rightarrow |{}^2S_{1/2}(F), n_r, m'_\ell, m'_F\rangle$  with  $m_\ell \neq m'_\ell$ , an optical square pulse which breaks the cylindrical symmetry of the QR is required. The electric field of the LG pulse is

$$\begin{aligned} \mathbf{E}_e(\mathbf{r}, t) = &\frac{\mathbf{e}_y}{2} [u_{l_e,0}(\mathbf{r}) + u_{-l_e,0}(\mathbf{r})] \cos(k_e z) \Theta(t, \tau - t) e^{-i\omega_e t} \\ &+ \text{c.c.}, \end{aligned}$$

where  $k_e = \omega_e/c$  is the wave number of the LG pulse,  $l_e$  is an orbital angular momentum of the LG pulse, and  $u_{l_e,0}(\mathbf{r})$  is given by Eq. (2). We choose the waist radii of the LG pulse  $w_e$  and the LG beam waist  $w_0$ , and their orbital angular momenta  $l_e$  and  $l$ , such that  $w_e\sqrt{|l_e|/2} = w_0\sqrt{|l|/2}$ . Interaction of the atoms with the LG pulse is given by the Hamiltonian

$$H_e = -\mathbf{p} \cdot \mathbf{E}_e(\mathbf{r}, t), \quad (20)$$

where  $\mathbf{p}$  is the atomic electric dipole operator.

Let us derive the effective Hamiltonian describing Rabi oscillations for the QR in the  $m_\ell$  and  $m'_\ell = m_\ell + 2l_e$  states. For this purpose, we assume that the low-energy states of the trapped atom are  $|{}^2S_{1/2}(1/2), n_r, m_\ell, m_F\rangle$  and  $|{}^2S_{1/2}(1/2), n_r, m'_\ell, m_F\rangle$  states with the electronic configuration  ${}^2S_{1/2}(F=1/2)$ , magnetic quantum number  $m_F = \pm 1/2$ , and the motion of the center of mass parametrized by the radial quantum number  $n_r$  and the orbital quantum number  $m_\ell$  and  $m'_\ell$ . High-energy states are  $|{}^2S_{1/2}(3/2), n_r, m_\ell, m_F\rangle$  and  $|{}^2S_{1/2}(3/2), n_r, m'_\ell, m_F\rangle$  with electronic configuration  ${}^2S_{1/2}(F=3/2)$ ,  $m_F = \pm 1/2$ , radial quantum number  $n_r$ , and the orbital quantum number  $m_\ell$  and  $m'_\ell$ , as well as  $|{}^2P_{3/2}, n_r, m'_\ell, m_F\rangle$  with electronic configuration  ${}^2P_{3/2}$ , radial quantum number  $n_r$ , orbital quantum number  $m'_\ell = m_\ell + l_e$ , and  $m_F = \pm 1/2$ . In this section, we use the following basis,

$$|0\rangle = |{}^2S_{1/2}(1/2), n_r, m_\ell, m_F\rangle, \quad (21a)$$

$$|1\rangle = |{}^2S_{1/2}(1/2), n_r, m_\ell + 2l_e, m_F\rangle, \quad (21b)$$

$$|2\rangle = e^{i\omega_p t} |{}^2S_{1/2}(3/2), n_r, m_\ell, m_F\rangle, \quad (21c)$$

$$|3\rangle = e^{i\omega_p t} |{}^2S_{1/2}(3/2), n_r, m_\ell + 2l_e, m_F\rangle, \quad (21d)$$

$$|4\rangle = e^{i\omega_e t} |{}^2P_{3/2}, n_r, m_\ell + l_e, m_F\rangle. \quad (21e)$$

The “nonperturbed” Hamiltonian of the trapped atom without the pump, Stokes, and LG pulses is given by the matrix elements,

$$\langle v | H_0 | v' \rangle = \varepsilon_v \delta_{v,v'}, \quad (22)$$

where  $v, v' = 0, 1, 2, 3, 4$ , and

$$\begin{aligned} \varepsilon_0 &= \varepsilon_r(n_r, m_\ell), \quad \varepsilon_1 = \varepsilon_r(n_r, m_\ell + 2l_e), \quad \varepsilon_2 = \hbar\Delta_{\text{hf}}, \\ \varepsilon_3 &= \hbar\Delta_{\text{hf}} + \varepsilon_r(n_r, m_\ell + 2l_e), \quad \varepsilon_4 = \hbar\Delta_e. \end{aligned} \quad (23)$$

The energy of the QR,  $\varepsilon_r(n_r, m_\ell)$ , is found from Eq. (13).  $\Delta_{\text{hf}} = \omega_p - \varepsilon_{\text{hf}}/\hbar$  and  $\Delta_e = \omega_e - \varepsilon_e/\hbar$  are the detuning of the pump and optical frequencies from the resonant frequencies of the quantum transitions  $|0\rangle \rightarrow |3\rangle$  and  $|0\rangle \rightarrow |4\rangle$ , respectively.

The nontrivial matrix elements of  $H_p$ ,  $H_s$ , and  $H_e$  in Eqs. (19) and (20) are

$$\begin{aligned} \langle 0|H_\mu|2\rangle &= \langle 1|H_\mu|3\rangle \\ &= g\mu_B B_\mu \langle {}^2S_{1/2}(1/2), m_F | S_y | {}^2S_{1/2}(3/2), m_F \rangle \\ &= \frac{\sqrt{2}}{3} g\mu_B B_\mu e^{i(\omega_\mu - \omega_p)t} m_F, \end{aligned} \quad (24a)$$

$$\begin{aligned} \langle 0|H_e|4\rangle &= \langle 1|H_e|4\rangle = \frac{1}{2} [u_{l_e,0}(r_l, 0, 0) + u_{-l_e,0}(r_l, 0, 0)] \\ &\quad \times \langle {}^2S_{1/2}, m_F | p_y | {}^2P_{3/2}, m_F \rangle, \end{aligned} \quad (24b)$$

where  $|{}^2S_{1/2}(F), m_F\rangle$  are the wave functions of the ground  ${}^2S_{1/2}$  state atom,  $|{}^2P_{3/2}, m_F\rangle$  are the state wave functions of the excited  ${}^2P_{3/2}$  state atom,  $m_F$  is the projection of  $\mathbf{F}$  on the  $y$  axis, and  $u_{l_e,0}(r, \phi, z)$  are given by Eq. (2).

#### A. Adiabatic elimination of the ${}^2S_{1/2}(F = 3/2)$ hyperfine state

As a first step, we apply the following unitary transformations,

$$\begin{aligned} |\psi_0\rangle &= u_b|0\rangle - v_b|2\rangle, & |\psi_1\rangle &= u_b|1\rangle - v_b|3\rangle, \\ |\psi_2\rangle &= v_b^*|0\rangle + u_b|2\rangle, & |\psi_3\rangle &= v_b^*|1\rangle + v_b|3\rangle, \end{aligned}$$

and  $|\psi_4\rangle = |4\rangle$ , where

$$v_b = \frac{\sqrt{2}}{3} \frac{g\mu_B(B_p + B_s e^{-i\omega_{ps}})}{\hbar\Delta_{\text{hf}}}, \quad u_b = \sqrt{1 - |v_b|^2}, \quad (25)$$

and  $\omega_{ps} = \omega_p - \omega_s$ . We assume here that  $|v_b| \ll 1$  and keep terms up to  $v_b^2$ , and neglect  $v_b^n$  with  $n \geq 3$ . This transformation makes  $H_0 + H_p + H_s$  diagonal,

$$\langle \psi_n | H_0 + H_p + H_s | \psi_{n'} \rangle = \tilde{\epsilon}_n \delta_{n,n'},$$

where

$$\begin{aligned} \tilde{\epsilon}_0 &= \epsilon_r(n_r, m_\ell) - \hbar\Delta_{\text{hf}}|v_b|^2, \\ \tilde{\epsilon}_1 &= \epsilon_r(n_r, m_\ell + 2l_e) - \hbar\Delta_{\text{hf}}|v_b|^2, \\ \tilde{\epsilon}_2 &= \hbar\Delta_{\text{hf}}(1 + |v_b|^2), \\ \tilde{\epsilon}_3 &= \hbar\Delta_{\text{hf}}(1 + |v_b|^2) + \epsilon_r(n_r, m_\ell + 2l_e), \\ \tilde{\epsilon}_4 &= \hbar\Delta_e. \end{aligned}$$

The matrix elements of  $H_e$  are

$$\begin{aligned} h_e &\equiv \langle \psi_0 | H_e | \psi_4 \rangle = \langle \psi_1 | H_e | \psi_4 \rangle \\ &= \frac{1}{2} [u_{l_e,0}(r_l, 0, 0) + u_{-l_e,0}(r_l, 0, 0)] \\ &\quad \times \langle {}^2S_{1/2}, m_F | p_x | {}^2P_{3/2}, m_F \rangle \left(1 - \frac{|v_b|^2}{2}\right), \end{aligned} \quad (26)$$

where  $u_{l_e,0}(r, \phi, z)$  is given by Eq. (2).

#### B. Adiabatic elimination of the ${}^2P_{3/2}$ excited state

In a second step, we apply the following unitary transformations,

$$\begin{aligned} |\tilde{\psi}_0\rangle &= u_g|\psi_0\rangle - \frac{v_e^2}{2}|\psi_1\rangle - v_e|\psi_4\rangle, \\ |\tilde{\psi}_1\rangle &= -\frac{v_e^2}{2}|\psi_0\rangle + u_g|\psi_1\rangle - v_e|\psi_4\rangle, \\ |\tilde{\psi}_4\rangle &= v_e|\psi_0\rangle + v_e|\psi_1\rangle + u_e|\psi_4\rangle, \end{aligned}$$

where

$$v_e = \frac{\hbar_e}{\Delta_e}, \quad u_g = \sqrt{1 - |v_e|^2}, \quad u_e = \sqrt{1 - 2|v_e|^2}.$$

We assume here that  $|v_e| \ll 1$  and keep terms up to  $v_e^2$  and neglect terms proportional to  $v_e^n$  with  $n \geq 3$ . Then the transformed Hamiltonian  $H = H_0 + H_p + H_s + H_e$  is given by the matrix elements,

$$\langle \tilde{\psi}_v | H | \tilde{\psi}_{v'} \rangle = (\epsilon_n - \hbar\Delta_{\text{hf}}|v_b|^2)\delta_{v,v'} - \frac{2|h_e|^2}{\hbar\Delta_e},$$

$$\langle \tilde{\psi}_4 | H | \tilde{\psi}_4 \rangle = \hbar\Delta_e + \frac{4|h_e|^2}{\hbar\Delta_e},$$

$$\langle \tilde{\psi}_v | H | \tilde{\psi}_4 \rangle = 0,$$

where  $v, v' = 0, 1$  and  $\epsilon_v$  are given by Eq. (23).

Omitting the high-energy state  $|\tilde{\psi}_4\rangle$ , we get the two-level effective Hamiltonian  $\mathcal{H}$  describing Rabi oscillations,

$$\mathcal{H} = \begin{pmatrix} \epsilon_r(n_r, m_\ell) & -2|h_e|^2/(\hbar\Delta_e) \\ -2|h_e|^2/(\hbar\Delta_e) & \epsilon_r(n_r, m_\ell + 2l_e) \end{pmatrix}, \quad (27)$$

where we shift the chemical potential by adding the term

$$\left(\Delta_{\text{hf}}|v_b|^2 + \frac{2|h_e|^2}{\Delta_e}\right) \begin{pmatrix} 1 & 0 \\ 0 & 1 \end{pmatrix}.$$

Taking into account Eqs. (26) and (25), we get

$$\begin{aligned} \frac{2|h_e|^2}{\hbar\Delta_e} &= \frac{\alpha(\omega_e)}{2} |u_{l_e,0}(r_l, 0, 0) + u_{-l_e,0}(r_l, 0, 0)|^2 \\ &\quad \times \left\{ 1 - \frac{1}{3} \frac{g^2 \mu_B^2}{\hbar^2 \Delta_{\text{hf}}^2} [B_p^2 + B_s^2 + 2B_p B_s \cos(\omega_{ps}t)] \right\}. \end{aligned} \quad (28)$$

On the right-hand side of Eq. (28) there are time-independent and time-dependent terms. The former can be considered as weak perturbation which does not contribute to the Rabi oscillations, whereas the second term gives rise to Rabi oscillations. The off-diagonal part of the Hamiltonian (27) after omitting the time-independent terms gives us the Rabi oscillations between the QR states  $|n_r, m_\ell\rangle$  and  $|n_r, m_\ell + 2l_e\rangle$ . Combining all the initial QR states  $|n_r, m_\ell\rangle$ , we get the Rabi oscillation Hamiltonian in the form

$$\begin{aligned} \mathcal{H}(t) &= \sum_{n_r, m_\ell} \epsilon_r(n_r, m_\ell) |n_r, m_\ell\rangle \langle n_r, m_\ell| \\ &\quad - 2\mathcal{V} \cos(\omega_{ps}t) \Theta(t, \tau - t) \\ &\quad \times \sum_{n_r, m_\ell} (|n_r, m_\ell\rangle \langle n_r, m_\ell + 2l_e| + \text{H.c.}). \end{aligned} \quad (29)$$

Hereafter, we use the notations

$$|n_r, m_\ell\rangle \equiv |{}^2S_{1/2}(1/2), n_r, m_\ell, m_F\rangle$$

for the QR wave functions. The coupling  $\mathcal{V}$  is

$$\mathcal{V} = \frac{\mathcal{V}_e \mathcal{V}_b}{\hbar\Delta_{\text{hf}}},$$

where

$$\mathcal{V}_b = \frac{g^2 \mu_B^2 B_p^{(0)} B_s^{(0)}}{3\hbar\Delta_{\text{hf}}}, \quad \mathcal{V}_e = \frac{4\alpha(\omega_e) P_e l_e^l e^{-l_e}}{\pi l_e! w_c^2 c}.$$

$P_e$  and  $w_e$  are the power and the beam waist of the LG pulse, and  $B_p^{(0)}$  and  $B_s^{(0)}$  are the magnetic field strengths of the pump and Stokes microwave pulses. The subscript  $e$  indicates the electric dipole interaction of the atom with the LG pulse, and the subscript  $b$  indicates the magnetic dipole interaction of the atoms with the pump and Stokes microwave pulses. The detuning  $\Delta_{\text{hf}}$  of the pump pulse frequency from the  ${}^2S_{1/2}(F = 1/2) \rightarrow {}^2S_{1/2}(F = 3/2)$  quantum transition frequency greatly exceeds the frequency  $\omega_{m_\ell+2l_e, m_\ell}$  of the  $|m_\ell\rangle \rightarrow |m_\ell + 2l_e\rangle$  quantum transition,  $|\Delta_{\text{hf}}| \gg \omega_{m_\ell+2l_e, m_\ell}$ , hence we can assume that  $\omega_p$  and  $\omega_s$  have the same detuning  $\Delta_{\text{hf}}$  from resonance. Details of the Raman scattering used to measure the energy differences of the QR states are presented in Ref. [1].

### C. Rabi oscillations in the inertial frame

With the QR initially in the ground state  $|n_r = 0, m_\ell = 0\rangle$ , subject it to Raman pulses of duration  $\tau$  and generalized Rabi frequency  $\Omega_R = 2\sqrt{2}\mathcal{V}/\hbar$ , such that  $\Omega_R\tau \approx \pi$ . In the rotating-wave approximation [21–24], the temporal evolution of a single QR wave function is given by  $|\Psi(\tau)\rangle = e^{-i\mathcal{H}_R\tau/\hbar}|0, 0\rangle$ , where  $\mathcal{H}_R$  is the Hamiltonian [see Eq. (29)]

$$\mathcal{H}_R = \hbar \begin{pmatrix} 0 & \Omega_R\sqrt{2}/4 & \Omega_R\sqrt{2}/4 \\ \Omega_R\sqrt{2}/4 & -\delta & 0 \\ \Omega_R\sqrt{2}/4 & 0 & -\delta \end{pmatrix}, \quad (30)$$

where the Rabi frequency is

$$\Omega_R = \frac{2\sqrt{2}\mathcal{V}}{\hbar}, \quad (31)$$

$\delta = \omega_{ps} - \omega_{0,2l_e}(0)$  is the detuning of  $\omega_{ps}$  from the resonant frequency  $\omega_{0,2l_e}$ , and the basis vectors are

$$|0, 0\rangle = \begin{pmatrix} 1 \\ 0 \\ 0 \end{pmatrix}, \quad |0, 2l_e\rangle = \begin{pmatrix} 0 \\ 1 \\ 0 \end{pmatrix}, \quad |0, -2l_e\rangle = \begin{pmatrix} 0 \\ 0 \\ 1 \end{pmatrix}.$$

The probability of finding the quantum rotor in the excited state  $|0, 2l_e\rangle$  or  $|0, -2l_e\rangle$  is

$$\begin{aligned} P_0(\delta, \Omega_R) &= |\langle 2l_e|\Psi(\tau)\rangle|^2 + |\langle -2l_e|\Psi(\tau)\rangle|^2 \\ &= \frac{\Omega_R^2}{\Omega_R^2 + \delta^2} \sin^2\left(\frac{\tau}{2}\sqrt{\Omega_R^2 + \delta^2}\right). \end{aligned} \quad (32)$$

$P_0(\delta, \Omega_R)$  has a peak,  $P_0(0, \Omega_R) = 1$  at  $\delta = 0$ . The peak half width at half maximum is  $1.732\Omega_R$ .

With  $N = 2j_{\text{max}} + 1$  atoms singly occupying the sites with  $|j| \leq j_{\text{max}}$ , the detuning of  $\omega_{ps}$  from the resonant frequency of the  $j$ th quantum rotor is  $\delta_j = \delta + 4L^2 j^2 \{\omega_0[r_l(0)] - \omega_0[r_l(z_j)]\}$ , where  $\delta$  is the detuning of  $\omega_{ps}$  from the resonant frequency of the  $j = 0$  QR,  $\omega_0[r_l(z)] = \hbar/[2Mr_l^2(z_j)]$  is the rotational frequency, and  $r_l(z_j)$  is the radius of the classical circular trajectory. As a result, the peak in the probability to find a QR in the final state is shifted and broadened. The probability to find a QR in the final state is

$$P(\delta, \Omega_R) = \frac{1}{2j_{\text{max}} + 1} \sum_{j=-j_{\text{max}}}^{j_{\text{max}}} P_0(\delta_j, \Omega_R). \quad (33)$$

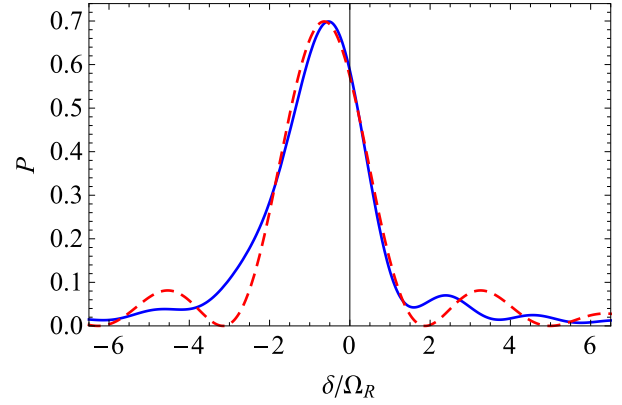


FIG. 4. The probability  $P$  in Eq. (33) for absorption of a pump photon and stimulated reemission of a Stokes photon with QRs quantum transition from state  $|n_r = 0, m_\ell = 0\rangle$  to  $(|0, 50\rangle + |0, -50\rangle)/\sqrt{2}$  as a function of the difference  $\omega_{ps} = \omega_p - \omega_s$  of the pump and Stokes frequencies  $\omega_p$  and  $\omega_s$  (solid blue curve). The dashed red curve shows the fit of  $P(\delta, \Omega_R)$  obtained as explained in the text.

Figure 4 shows  $P(\delta, \Omega_R)$  of Eq. (33) plotted as a function of  $\delta$ , for rotational frequency  $\omega_0 = 21.13 \text{ s}^{-1}$ , corresponding to an LG beam with  $w_0 = 10 \mu\text{m}$  and  $l = 5$ , Rabi frequency  $\Omega_R = 3.142 \text{ s}^{-1}$ , pulse duration  $\tau \approx \pi/\Omega_R = 1 \text{ s}$ ,  $j_{\text{max}} = 80$ ,  $m_\ell = 0$ , and  $m'_\ell = 50$ . The solid blue curve shows that  $P(\delta, \Omega_R)$  has a peak,  $P_{\text{max}} = P(\delta_{\text{max}}, \Omega_R) = 0.6989$ , at  $\delta_{\text{max}} = -0.5374\Omega_R$ . The dashed red curve shows the fitting of  $P(\delta, \Omega_R)$  by the function  $P(\delta, \Omega_R) \approx \mathcal{A}P_0(\delta - \delta_0, \tilde{\Omega}_R)$  with  $\mathcal{A} = 0.67987$  and  $P_0$  is given by Eq. (32) with  $\delta_0 = -0.64002\Omega_R$ ,  $\tilde{\Omega}_R = 1.4865\Omega_R$ . Note that  $\delta_{\text{max}} \neq \delta_0$ . This is partly because the function  $P(\delta, \Omega_R)$  is not symmetric with respect to the inversion  $\delta - \delta_{\text{max}} \rightarrow -(\delta - \delta_{\text{max}})$ , whereas the function  $P_0(\delta, \Omega_R) = P_0(-\delta, \Omega_R)$  is symmetric.

In addition, different transition frequencies obtained from the  $m_\ell \rightarrow m'_\ell$  transition for different  $z_j$  result in broadening of the peak of  $P(\delta, \Omega_R)$  in Eq. (33). For example, when the beam waist  $w_0$  is  $10 \mu\text{m}$ ,  $\Omega_R = 3.142 \text{ s}^{-1}$ , and when the sites with  $|j| \leq 80$  are singly occupied and thus  $N = 161$ , the resulting peak half width at half maximum is  $1.732\tilde{\Omega}_R = 2.575\Omega_R$  instead of  $1.732\Omega_R$  for a single QR (see Fig. 4).

We now show that trapped ground-state QRs in an LG beam can be used as extremely accurate rotation sensors.

### V. ROTATION SENSOR

Consider a QR in a noninertial frame rotating with angular velocity  $\mathbf{\Omega} = \Omega \mathbf{e}_z$  as illustrated in Fig. 5. Then, an additional term is needed in the Hamiltonian,

$$H_\Omega = \hbar\Omega\ell_z, \quad (34)$$

where  $\ell_z = -i\partial_\phi$  is the QR orbital momentum operator. The Hamiltonian (34) lifts the symmetry under the transformation  $(x, y, z) \rightarrow (-x, y, z)$  but not the rotational symmetry about the  $z$  axis. As a result,  $m_\ell$ , the eigenvalue of  $\ell_z$ , is a good quantum number, and the energy levels  $\epsilon_{m_\ell}$  of the rotational motion become  $\epsilon_{m_\ell}(\Omega) = \epsilon_{m_\ell} + \hbar\Omega m_\ell$ . Hereafter we use the inequalities (14) and restrict ourselves by considering the quantum states with  $n_z = n_r = 0$ . Moreover, using the

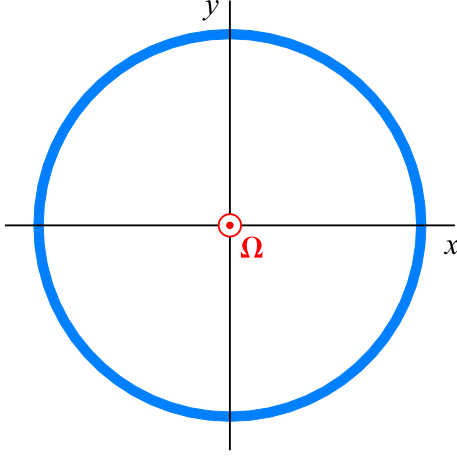


FIG. 5. QR (blue ellipse) subject to a rotation with angular velocity  $\Omega = \Omega \mathbf{e}_z$ .

inequalities (14), we approximate the rotational energies as  $\epsilon_{m_\ell} = m_\ell^2 C(r_l)$ , where  $r_l$  is given by Eq. (6).

Let us consider the frequencies of the quantum transitions between the quantum states  $|m_\ell\rangle$  and  $|m'_\ell\rangle$  with  $m_\ell = 0, \pm 1$  and  $m'_\ell = m_\ell \pm 2l_e$ . We have six spectral lines with frequencies  $\omega_{m_\ell, m_\ell \pm 2l_e}(\Omega)$  which are convenient to order as follows:  $\omega_{0, \pm 2l_e}(\Omega)$ ,  $\omega_{\pm 1, \pm(1+2l_e)}(\Omega)$ , and  $\omega_{\pm 1, \pm(1-2l_e)}(\Omega)$ . The frequencies of the quantum transitions between  $|0, \zeta m_\ell\rangle$  and  $|0, \zeta m_\ell + 2\zeta l_e\rangle$  are

$$\omega_{m_\ell, m_\ell + 2\zeta l_e}(\Omega) = 4l_e(l_e + m_\ell)\omega_0 + 2\zeta l_e \Omega, \quad (35)$$

where  $\zeta = \pm 1$ , and the rotational frequency is  $\omega_0 = C(r_l)/\hbar$ . Hence, when  $\Omega = 0$ ,  $\omega_{m_\ell, m_\ell + 2l_e}(0) = \omega_{-m_\ell, -(m_\ell + 2l_e)}(0)$ . One can measure the three spectral lines  $\omega_{0, 2l_e}(0) = \omega_{0, -2l_e}(0)$ ,  $\omega_{1, 1+2l_e}(0) = \omega_{-1, -1+2l_e}(0)$ , and  $\omega_{1, 1+2l_e}(0) = \omega_{-1, -1-2l_e}(0)$ . When  $\Omega \neq 0$ , the degeneracy of the spectral lines is lifted and the splitting is

$$\Delta\omega_{m_\ell, m_\ell + 2l_e} \equiv \omega_{m_\ell, m_\ell + 2l_e}(\Omega) - \omega_{-m_\ell, -m_\ell - 2l_e}(\Omega) = 4l_e \Omega. \quad (36)$$

Equation (36) shows that measuring the splitting of the spectral lines (35) can be used to determine  $\Omega$ . The frequency splitting (36) due to  $\Omega$  distinguishes between clockwise and counterclockwise rotations. All the spectral lines have the same splittings. Hence, the frequencies satisfy the periodic condition  $\omega_{m_\ell + m_\Omega, m_\ell + m_\Omega + 2l_e}(\Omega - 2m_\Omega \omega_0) = \omega_{m_\ell, m_\ell + 2l_e}(\Omega)$ , where  $m_\Omega$  is an integer.

#### A. Rabi oscillations in the rotating frame

We consider here Rabi oscillations of the QR in the frame of reference rotating with the angular velocity  $\Omega$ . In this case, the frequencies of the quantum transitions  $|0, 0\rangle \rightarrow |0, \pm 2l_e\rangle$  are given by Eq. (35). The Hamiltonian in Eq. (30) for  $\omega_{ps} = \omega_{0, 2l_e}(0)$  and  $\Omega_R \tau = \pi$  takes the form

$$\mathcal{H}_R(\Omega) = \hbar \begin{pmatrix} 0 & \Omega_R \sqrt{2}/4 & \Omega_R \sqrt{2}/4 \\ \Omega_R \sqrt{2}/4 & \Omega_{l_e}/2 & 0 \\ \Omega_R \sqrt{2}/4 & 0 & -\Omega_{l_e}/2 \end{pmatrix}, \quad (37)$$

where  $\Omega_{l_e} = 4l_e \Omega$ , and the Rabi frequency  $\Omega_R$  is given by Eq. (31). The probability of finding the quantum rotor in the

excited state  $|0, 2l_e\rangle$  or  $|0, -2l_e\rangle$  is

$$P(\Omega, \Omega_R) = \frac{4\Omega_R^2}{\tilde{\Omega}_R(\Omega_{l_e})} \sin^2\left(\frac{\pi}{4} \frac{\Omega_R}{\tilde{\Omega}_R(\Omega_{l_e})}\right) \times \left[1 - \frac{\Omega_R^2}{\tilde{\Omega}_R(\Omega_{l_e})} \sin^2\left(\frac{\pi}{4} \frac{\Omega_R}{\tilde{\Omega}_R(\Omega_{l_e})}\right)\right], \quad (38)$$

where

$$\tilde{\Omega}_R(\Omega_{l_e}) = \sqrt{\Omega_R^2 + \Omega_{l_e}^2}.$$

The probability  $P(\Omega, \Omega_R)$  has its maximum,  $P(0, \Omega_R) = 1$ , at  $\Omega = 0$ , and for  $\Omega \neq 0$ ,  $P(\Omega, \Omega_R) < 1$ . Measuring  $P(\Omega, \Omega_R)$  and applying Eq. (38), one can find  $\Omega$ .

#### B. Rotation measurement accuracy estimate

When QRs are placed in a noninertial frame rotating with angular velocity  $\Omega = \Omega \mathbf{e}_z$ , they can be used as a highly accurate rotation sensor to determine  $\Omega$ . Here, we derive the uncertainty in the angular velocity due to (1) the uncertainty of the pump and Stokes frequencies, (2) the Rabi frequency fluctuations, and (3) the shot noise in the pump and Stokes pulses.

##### 1. Uncertainty due to fluctuation of the pump and Stokes frequencies

Note that Eq. (36) does not contain any information regarding the optical potential, the laser frequency, or the intensity. Therefore the uncertainty of  $\Omega$ ,  $\delta\Omega$ , is determined solely by uncertainty  $\delta\omega$  of the pump and Stokes frequencies,

$$\delta\Omega_{ps} = \frac{1}{\sqrt{N}} \frac{\delta\omega}{4l_e}. \quad (39)$$

Here,  $N = 2j_{\max} + 1$  is the number of atoms singly occupying the sites with  $|j| \leq j_{\max}$ ,  $\delta\omega = \sqrt{\delta\omega_p^2 + \delta\omega_s^2}$ , and  $\delta\omega_p$  and  $\delta\omega_s$  are the uncertainties of the pump and Stokes frequencies. For  ${}^6\text{Li}$  atoms, we take  $\omega_p \gtrsim \omega_s \approx 1.43 \times 10^9 \text{ s}^{-1}$ . The Allan variance estimate of Ref. [25] for the pump and Stokes pulses is  $\delta\omega_p \approx \delta\omega_s \approx 3 \times 10^{-16} \omega_p$  for an integration time  $\tau = 40 \text{ s}$ . For a  $\pi$  pulse duration of 60 s,  $\delta\omega$  is calculated to be  $\delta\omega = \sqrt{2} \delta\omega_p \approx 6.08 \times 10^{-7} \text{ s}^{-1}$ . This pulse duration is longer than the integration time 40 s in Ref. [25], but shorter than the lifetime of  ${}^6\text{Li}$  atoms trapped in an optical lattice which is reported in Ref. [26] to be more than 70 s. The lifetime of Rb atoms trapped in an optical lattice is studied in Ref. [10], which showed that there is an initial period of 20 s during which the atom loss is minimal, and then the population decays exponentially with a 62 s time constant.

From Eq. (39) we see that the larger the orbital angular momentum  $l_e$  of the LG pulse, the smaller is the  $\delta\Omega$ . When  $l_e = 25$  and  $j_{\max} = 80$ ,

$$\delta\Omega = 4.8 \times 10^{-10} \text{ s}^{-1}. \quad (40)$$

##### 2. Uncertainty due to Rabi frequency fluctuation

Fluctuation in  $\omega_p$  and  $\omega_s$  results in fluctuations in  $\Delta_{\text{hf}}$ , and as a result, in an uncertainty  $\delta\Omega_R$  of the Rabi frequency in

Eq. (31),

$$\delta\Omega_R = \frac{\Omega_R}{\Delta_{\text{hf}}} \delta\omega_p, \quad (41)$$

where we approximate  $\delta\omega_s \approx \delta\omega_p$ . Consider a fluctuation of  $P_0(\delta, \Omega_R)$  due to fluctuations of  $\delta$  and  $\Omega_R$ ,

$$P_0(\delta \pm \delta\omega_R, \Omega_R \pm \delta\Omega_R) = P_0(\delta, \Omega_R) - \frac{\delta\omega^2}{\Omega_R^2} - \frac{\pi^2}{4} \frac{\delta\Omega_R^2}{\Omega_R^2}. \quad (42)$$

The uncertainty  $\delta\omega_R$  of  $\delta = \omega_{ps} - \omega_{0,2\ell}$  due to fluctuation of  $\Omega_R$  is found from the equation

$$P_0(\pm\delta\omega_R, \Omega_R) = P_0(0, \Omega_R \pm \delta\Omega_R).$$

Taking into account Eq. (42), we find

$$\frac{\delta\omega_R^2}{\Omega_R^2} = \frac{\pi^2}{4} \frac{\delta\Omega_R^2}{\Omega_R^2},$$

which gives the solution

$$\delta\omega_R = \frac{\pi}{2} \delta\Omega_R = \frac{\pi}{2} \frac{\Omega_R}{\Delta_{\text{hf}}} \delta\omega_p, \quad (43)$$

where we take into account Eq. (41).

Knowing  $\delta\omega_R$ , we can calculate the uncertainty  $\delta\Omega_\omega$  of the angular velocity due to fluctuation of the Rabi frequency,

$$\delta\Omega_\omega = \frac{\pi}{2\sqrt{N}} \frac{\Omega_R}{\Delta_{\text{hf}}} \frac{\delta\omega_p}{4\ell_e}, \quad (44)$$

where  $N$  is the number of the quantum rotors. Comparing Eqs. (40) and (44), one can see that

$$\frac{\delta\Omega_\omega}{\delta\Omega_{ps}} = \frac{\pi}{2\sqrt{2}} \frac{\Omega_R}{\Delta_{\text{hf}}} \ll 1.$$

When  $\Omega_R = 3.142 \text{ s}^{-1}$  and  $\Delta_{\text{hf}} = 1.26 \times 10^8 \text{ s}^{-1}$ , the ratio  $\delta\Omega_\omega/\delta\Omega_{ps} = 2.77 \times 10^{-8}$  is really small.

### 3. Uncertainty due to shot noise in the pump and Stokes pulses

Another source of uncertainty arises from the shot noise in the Stokes, pump, and kick pulses. Shot noise results in fluctuations in the position and amplitude of the population oscillations of the Ramsey fringes because of fluctuation of the Rabi frequencies, and thus in the uncertainty in the phase  $\phi_R = \Omega_R \tau_\pi$ ,

$$\phi_R = \pi \pm \delta\phi_{\text{sn}}, \quad (45)$$

where

$$\delta\phi_{\text{sn}} \approx \pi \left( \frac{1}{\sqrt{N_p}} + \frac{1}{\sqrt{N_s}} \right),$$

and  $N_p$  and  $N_s$  are the photon number in the pump and Stokes pulses during the pulse time  $\tau_\pi = \pi/\Omega_R$ . Thus fluctuation in the Rabi frequency  $\Omega_R$  due to the shot noise is

$$\delta\Omega_R = \Omega_R \left( \frac{1}{\sqrt{N_p}} + \frac{1}{\sqrt{N_s}} \right).$$

In order to find the uncertainty  $\delta\Omega_{\text{sn}}$  in the angular velocity due to the shot noise, we apply the technique developed in

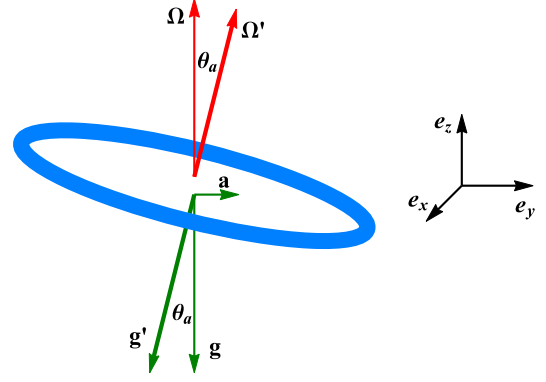


FIG. 6. Elimination of the in-plane acceleration  $\mathbf{a}$  by inclining the QRs. Here,  $\mathbf{g} = -g\mathbf{e}_z$  is the acceleration due to gravity,  $\boldsymbol{\Omega}$  is the angular velocity, and  $\mathbf{g}' = \mathbf{g} - \mathbf{a}$  is the total acceleration, where  $\mathbf{e}_x$ ,  $\mathbf{e}_y$ , and  $\mathbf{e}_z$  are unit vectors parallel to the  $x$ ,  $y$ , and  $z$  axes.  $\boldsymbol{\Omega}' = \Omega' \mathbf{e}'_z$ , where  $\Omega' = (\boldsymbol{\Omega} \cdot \mathbf{e}'_z)$  and the unit vector  $\mathbf{e}'_z$  is antiparallel to  $\mathbf{g}'$ . The angle between  $\mathbf{g}$  and  $\mathbf{g}'$  is  $\theta_a$ . The blue ellipse is the QR placed in the plane perpendicular to  $\mathbf{g}'$ .

Eqs. (42)–(44) and get

$$\delta\Omega_{\text{sn}} = \frac{\pi}{2\sqrt{N}} \frac{\Omega_R}{4\ell_e} \left( \frac{1}{\sqrt{N_p}} + \frac{1}{\sqrt{N_s}} \right), \quad (46)$$

where  $N$  is the number of the quantum rotors. Comparing Eqs. (40) and (46), one can see that

$$\frac{\delta\Omega_{\text{sn}}}{\delta\Omega_{ps}} = \frac{\pi}{2\sqrt{2}} \frac{\Omega_R}{\delta\omega_p} \left( \frac{1}{\sqrt{N_p}} + \frac{1}{\sqrt{N_s}} \right) \ll 1.$$

Indeed, when the numbers of photons in the pump and Stokes pulses are  $N_p \sim N_s \sim 10^{29}$ , the Rabi frequency is  $\Omega_R = 3.142 \text{ s}^{-1}$ , and the fluctuation of the pump frequency is  $\delta\omega_p = 4.29 \times 10^{-7} \text{ s}^{-1}$ , the ratio  $\delta\Omega_{\text{sn}}/\delta\Omega_{ps} = 5.14 \times 10^{-8}$  is really small.

### C. Discriminating against in-plane acceleration

An additional term  $H_g = -M\mathbf{g} \cdot \mathbf{r}$  must be added into the QR Hamiltonian to model the effects of a gravitational field  $\mathbf{g}$  [1]. This preserves the rotational symmetry in the plane perpendicular to  $\mathbf{g}$  (the  $x$ - $y$  plane in Fig. 6), but lifts the rotational symmetry in the  $x$ - $z$  and  $y$ - $z$  planes. As a result, the QRs rotating in the  $x$ - $y$  plane clockwise and counterclockwise with the same quantum number  $|m_\ell|$  have the same energy. When the QRs are placed in the  $x$ - $z$  or  $y$ - $z$  plane (such that  $\mathbf{g}$  is in the plane of the QRs), the degeneracies of the quantum states  $|m_\ell\rangle$  and  $| -m_\ell\rangle$  are split and the splitting depends on  $m_\ell$ . Hence, placing the QRs in the  $x$ - $y$  plane, we obtain the energy splitting of the levels caused just by  $\Omega_z$ , the  $z$  component of the angular velocity  $\boldsymbol{\Omega}$ .

If an additional acceleration  $\mathbf{a}$  in the  $x$ - $y$  plane is present, there is an additional splitting of the degenerate QR ground state, and the frequency splitting in Eq. (36) becomes dependent on  $m_\ell$ . Hence, turn the plane of the QRs to be perpendicular to  $\mathbf{g}' = \mathbf{g} - \mathbf{a}$  so that the frequency splitting (36) is independent on  $m_\ell$ , and obtain the energy splitting

of the levels caused just by  $\Omega' = \mathbf{\Omega} \cdot \mathbf{e}'_z$ , where  $\mathbf{e}'_z$  is the unit vector along  $-\mathbf{g}'$ , as illustrated in Fig. 6.

## VI. SUMMARY AND CONCLUSION

Cold atoms trapped in a Laguerre-Gauss optical potential (5) are confined to circular rings (doughnuts) of radius  $r_l$  with centers on the axis of the Laguerre-Gauss beam, i.e., they are quantum rotors. Rings with one atom per site (to suppress spin-exchange collisions) can be used as highly accurate rotation sensors. We estimate the accuracy of the rotation sensor due to the fluctuations of the pump and Stokes frequencies and intensities (Rabi frequencies), and the shot noise of the

Stokes and pump pulses. We show that the main contribution to the rotation frequency uncertainty is due to the fluctuations of the pump and Stokes frequencies. When  $r_l = 15.81 \mu\text{m}$ , the accuracy obtained with  $N = 161$  atoms singly occupying the sites with  $|j| \leq 80$  is  $\delta\Omega = 4.8 \times 10^{-10} \text{ s}^{-1}$ . This is somewhat better than the accuracy  $\delta\Omega = 6.4 \times 10^{-10} \text{ s}^{-1}$  reported in Ref. [1]. Moreover, our rotation sensor accuracy is also better than  $\delta\Omega_{\text{NIST}} = 1 \text{ nrad s}^{-1}$  reported in Ref. [15].

## ACKNOWLEDGMENT

This work was supported in part by a grant from the DFG through the DIP program (FO703/2-1).

- 
- [1] I. Kuzmenko, T. Kuzmenko, Y. Avishai, and Y. B. Band, *Phys. Rev. A* **100**, 033415 (2019).
- [2] M. Babiker, D. L. Andrews, and V. E. Lembessis, *J. Opt.* **21**, 013001 (2019).
- [3] G. Goubau and F. Scherwing, *IRE Trans.* **9**, 248 (1961).
- [4] L. Allen, M. W. Beijersbergen, R. J. C. Spreeuw, and J. P. Woerdman, *Phys. Rev. A* **45**, 8185 (1992).
- [5] M. A. Clifford, J. Arlt, J. Courtial, and K. Dholakia, *Opt. Commun.* **156**, 300 (1998).
- [6] F. Pampaloni and J. Enderlein, [arXiv:physics/0410021](https://arxiv.org/abs/physics/0410021).
- [7] W. H. Carter and M. F. Aburdene, *J. Opt. Soc. Am. A* **4**, 1949 (1987).
- [8] L. Viverit, C. Menotti, T. Calarco, and A. Smerzi, *Phys. Rev. Lett.* **93**, 110401 (2004).
- [9] I. Bloch, J. Dalibard, and W. Zwerger, *Rev. Mod. Phys.* **80**, 885 (2008).
- [10] M. J. Gibbons, S. Y. Kim, K. M. Fortier, P. Ahmadi, and M. S. Chapman, *Phys. Rev. A* **78**, 043418 (2008).
- [11] Alternatively, one could consider a different configuration consisting of a red-detuned version of a trap developed by T. Kuga, Y. Torii, N. Shiokawa, T. Hirano, Y. Shimizu, and H. Sasada [*Phys. Rev. Lett.* **78**, 4713 (1997)], with an LG beam and two additional “plugging” laser beams which limit the atomic motion along the optical axis of the LG beam.
- [12] L. Allen, M. Babiker, W. K. Lai, and V. E. Lembessis, *Phys. Rev. A* **54**, 4259 (1996).
- [13] E. M. Wright, J. Arlt, and K. Dholakia, *Phys. Rev. A* **63**, 013608 (2000).
- [14] S. A. Kennedy, G. W. Biedermann, J. T. Farrar, T. G. Akin, S. Krzyzewski, and E. R. I. Abraham, *Opt. Commun.* **321**, 110 (2014).
- [15] I. Dutta, D. Savoie, B. Fang, B. Venon, C. L. Garrido Alzar, R. Geiger, and A. Landragin, *Phys. Rev. Lett.* **116**, 183003 (2016).
- [16] D. Savoie, M. Altorio, B. Fang, L. A. Sidorenkov, R. Geiger, and A. Landragin, *Sci. Adv.* **4**, 7948 (2018).
- [17] J. C. Fang and J. Qin, *Sensors* **12**, 6331 (2012).
- [18] G. W. Hoth, B. Pelle, S. Riedl, J. Kitching, and E. Donley, *Appl. Phys. Lett.* **109**, 071113 (2016).
- [19] N. F. Ramsey, *Phys. Rev.* **78**, 695 (1950).
- [20] F. Le Kien, P. Schneeweiss, and A. Rauschenbeutel, *Eur. Phys. J. D* **67**, 92 (2013).
- [21] R. Loudon, *The Quantum Theory of Light*, 3rd ed. (Oxford University Press, Oxford, U.K., 2000), p. 52.
- [22] Y. B. Band and Y. Avishai, *Quantum Mechanics with Applications to Nanotechnology and Information Science* (Elsevier, Oxford, U.K., 2013), p. 187.
- [23] T. Zanon-Willette, S. Almonacil, E. de Clercq, A. D. Ludlow, and E. Arimondo, *Phys. Rev. A* **90**, 053427 (2014).
- [24] Y. Wu and X. Yang, *Phys. Rev. Lett.* **98**, 013601 (2007).
- [25] N. R. Nand, J. G. Hartnett, E. N. Ivanov, and G. Santarelli, *IEEE Trans. Microwave Theory Tech.* **59**, 11 (2011).
- [26] S. Blatt, A. Mazurenko, M. F. Parsons, C. S. Chiu, F. Huber, and M. Greiner, *Phys. Rev. A* **92**, 021402(R) (2015).